*Journal of Sound and Vibration* (2000) **231**(5), 1289–1309
doi:10.1006/jsvi.1999.2731, available online at http://www.idealibrary.com on IDEAL®

# GROUND VIBRATION IN THE VICINITY OF A HIGH-SPEED MOVING HARMONIC STRIP LOAD

G. LEFEUVE-MESGOUEZ AND D. LE HOUÉDEC

*Ecole Centrale de Nantes, LMM, B.P.* 92101, 44072 *NANTES Cedex* 03, *France*

AND

A. T. PEPLOW

*Department of Mathematical Sciences, University of the West of England, Coldharbour Lane, Bristol, BS*16 1*QY, England*

(*Received* 5 *March* 1999, *in final form* 7 *October* 1999)

The transmission of vibrations over the surface of the ground, due to a high-speed moving, vertical harmonic strip load, is investigated theoretically. Consequently, the problem is essentially two-dimensional and the interior of the ground is modelled as an elastic half-space. The transformed solutions are obtained using the Fourier transform on the space variable. A study of a new damping model in the spatial wave-number domain is presented in Appendix A. Numerical results for the displacements on the surface are presented for loads moving with speeds up to and beyond the Rayleigh wave speed of the half-space.



## 1. INTRODUCTION

The problem of determining the response of a solid medium under the action of moving loads has received considerable attention in the past. Work in this area has been motivated by the need to determine the vibratory motion on the ground surface and at depth caused by moving vehicles. Moreover, high-speed trains are becoming increasingly popular and freight trains increasingly heavier. Combined with this fact and the observation that Rayleigh wave speeds are slower in soft soils, it is clear that the study of moving loads is important for environmental and geotechnical engineers.

The two-dimensional problem of the steady state motion of a static line load in an unbounded body was first considered by Eason *et al.* [1]. Eason [2], also studied the two-dimensional steady state problem for a uniform half-space, using Fourier transform methods. Cole and Huth [3], considered the same problem for a constant normal line load and obtained analytical forms for the solutions for the displacements, for the subsonic, transonic and supersonic cases, using a Helmholtz decomposition. Georgiadis and Barber [4], corrected the Cole and Huth solution for transonic regime. Fryba [5], also investigated the possibility of shocks in the ground due to a line load moving at constant speed at or beyond the Rayleigh wave

0022-460X/00/151289 + 21 $35.00/0 

speed. Keer [6], extended the study of the subsonic case to a moving harmonic line load with some numerical solutions. More recently, Gunaratne and Sanders [7], studied the response of a layered elastic medium to a moving strip load using a layer stiffness approach and viscous damping. De Barros and Luco [8], investigated the response of a layered viscoelastic half-space to a moving constant line load, and studied the stresses and strains. The transient motion for a line load which is suddenly applied on the ground and then moves with constant velocity has been studied by Payton [9]. The three-dimensional problem of a point load moving at constant speed on the ground demonstrating the possibility of shock formation in the ground has been studied by a number of authors, such as De Barros and Luco [10], Krylov [11] and Jones *et al.* [12].

In the present paper the transmission of vibrations due to a moving harmonic strip load rigidly attached to an elastic half-space is investigated. A two-dimensional model is considered to demonstrate the effect of a coherent line source as a pre-cursor to a three-dimensional model of a moving point source to be presented in a sequel. The results derived by Fourier transform are valid for any frequency and load speed. After evaluating the inverse Fourier transforms numerically, the values of displacements and the nature of the wavefront are calculated for different material parameters and depths of soil. For vibration and acoustic problems in unbounded domains it is necessary to consider a suitable damping model. For moving loads, in particular, a theoretical model requires careful attention. An original "modified" hysteretic damping model is investigated in Appendix A.

## 2. VIBRATION TRANSMISSION

The model considered is shown in Figure 1. The strip load has a length $2b$, and is aligned with respect to the $x_2$-axis. It rests on an homogeneous, isotropic, elastic half-space, with material properties $E$ (Young's modulus), $\rho$ (density) and $v$ (the Poisson ratio). First, we consider no energy losses within the ground (the material damping will be studied later). An harmonic vertical load acts uniformly over the strip and moves in the $x_1$-direction at constant speed, $c$. The model is two-dimensional.

The behaviour of the half-space is described by Navier's elastodynamic equations. In the absence of body forces, these can be written as

$$(\lambda + \mu)\nabla(\nabla \cdot \mathbf{u}) + \mu\nabla^2\mathbf{u} = \rho\ddot{\mathbf{u}}, \tag{1}$$

where $\lambda$ and $\mu$ are the Lamé constants, $\mathbf{u}$ is the vector of displacements, and the superscripts ($\ddot{}$) denote double differentiation with respect to time.

The stress–strain relations can be written as

$$\tau_{ij} = \lambda\varepsilon_{kk}\delta_{ij} + 2\mu\varepsilon_{ij}, \quad \text{where } \varepsilon_{ij} = \frac{1}{2}\left(\frac{\partial u_i}{\partial x_j} + \frac{\partial u_j}{\partial x_i}\right). \tag{2}$$

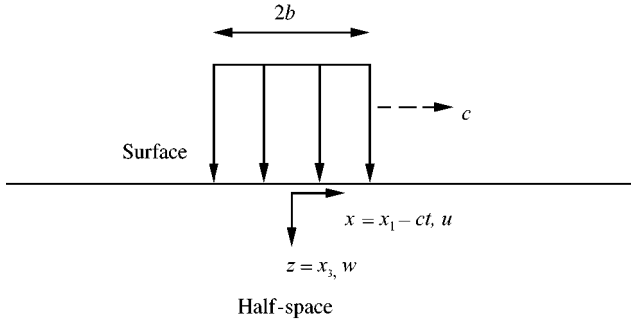


Figure 1. Geometry of model.

In equations (2), $\tau_{ij}$ are the stress components, $\varepsilon_{ij}$ are the strain components as defined, $\delta_{ij}$ is the Kronecker delta, $u_i$ and $x_i$ are the $i$th components of the vectors $(u_1, u_3)$ and $(x_1, x_3)$, respectively, and the summation convention applies. By introducing a Helmholtz decomposition in the equations of motion and the stress–strain relations, one obtains the following wave equations for the two-dimensional problem:

$$\left(\frac{\partial^2}{\partial x_1^2} - \frac{\partial^2}{\partial x_3^2}\right)\Phi - \frac{1}{c_1^2}\frac{\partial^2 \Phi}{\partial t^2} = 0, \qquad \left(\frac{\partial^2}{\partial x_1^2} - \frac{\partial^2}{\partial x_3^2}\right)\psi - \frac{1}{c_2^2}\frac{\partial^2 \psi}{\partial t^2} = 0 \tag{3}$$

with

$$u_1 = \frac{\partial \Phi}{\partial x_1} - \frac{\partial \psi}{\partial x_3}, \qquad u_3 = \frac{\partial \Phi}{\partial x_3} + \frac{\partial \psi}{\partial x_1}, \tag{4}$$

where $\Phi$ and $\psi$ are the Helmholtz potentials. The co-ordinates $(x_1, x_3)$ are the fixed frame of reference, $c_1$ and $c_2$ are, respectively, the $P$ and $S$ wave speeds, given by

$$c_1^2 = \frac{\lambda + 2\mu}{\rho} = \frac{E(1-\nu)}{\rho(1+\nu)(1-2\nu)}, \quad c_2^2 = \frac{\mu}{\rho} = \frac{E}{2\rho(1+\nu)}. \tag{5}$$

In terms of the scalar potentials, the boundary conditions for this problem are as follows:

(a) at $x_3 = 0$,

$$\sigma_{33} = \lambda \frac{\partial^2 \Phi}{\partial x_1^2} + (\lambda + 2\mu)\frac{\partial^2 \Phi}{\partial x_3^2} + 2\mu \frac{\partial^2 \psi}{\partial x_1 \partial x_3},$$

$$= \begin{cases} -P/2b\, e^{i\omega t}, & |x_1 - ct| < b, \\ 0, & \text{elsewhere}, \end{cases} \tag{6}$$

$$\tau_{13} = \left(2\frac{\partial^2 \Phi}{\partial x_1 \partial x_3} + \frac{\partial^2 \psi}{\partial^2 x_1} - \frac{\partial^2 \psi}{\partial^2 x_3}\right),$$

$$= 0. \tag{7}$$

(b) at $x_3 = \infty$, there are no reflections, which means that all wave motions are in the positive $x_3$-direction.

## 2.1. TRANSFORMED SOLUTION

### 2.1.1. *Change of variables*

If the motion is harmonic with frequency $\omega$ and moving at a speed $c$ in the $x_1$ direction, then introducing the moving co-ordinate, $x = x_1 - ct$, frame one can write:

$$u_1(x_1 - ct, x_3, t) = U(x, z, t) = u(x, z)\,\mathrm{e}^{\mathrm{i}\omega t}, \tag{8}$$

$$u_3(x_1 - ct, x_3, t) = W(x, z, t) = w(x, z)\,\mathrm{e}^{\mathrm{i}\omega t}, \tag{9}$$

$$\Phi(x_1 - ct, x_3, t) = \phi(x, z)\mathrm{e}^{\mathrm{i}\omega t}, \tag{10}$$

$$\psi(x_1 - ct, x_3, t) = \psi(x, z)\mathrm{e}^{\mathrm{i}\omega t}. \tag{11}$$

Thus, the derivatives are changed as follows:

$$\dot{\Phi} = (\mathrm{i}\omega\phi - c\phi_x)\mathrm{e}^{\mathrm{i}\omega t} \quad \text{and} \quad \ddot{\Phi} = (-\omega^2\phi - 2\mathrm{i}\omega c\phi_x + c^2\phi_{xx})\mathrm{e}^{\mathrm{i}\omega t}, \tag{12}$$

where the subscript $\phi_x$ denotes partial differentiation with respect to $x$. We can therefore re-write equation (3) as

$$\left(1 - \left(\frac{c}{c_1}\right)^2\right)\frac{\partial^2 \phi}{\partial x^2} + \frac{\partial^2 \phi}{\partial z^2} + 2\mathrm{i}\omega\frac{c}{c_1^2}\frac{\partial \phi}{\partial x} + \frac{\omega^2}{c_1^2}\phi = 0, \tag{13}$$

$$\left(1 - \left(\frac{c}{c_2}\right)^2\right)\frac{\partial^2 \psi}{\partial x^2} + \frac{\partial^2 \psi}{\partial z^2} + 2\mathrm{i}\omega\frac{c}{c_2^2}\frac{\partial \psi}{\partial x} + \frac{\omega^2}{c_2^2}\psi = 0. \tag{14}$$

The boundary conditions are changed by simply replacing $\Phi$ and $\psi$ with $\phi\mathrm{e}^{\mathrm{i}\omega t}$ and $\psi\mathrm{e}^{\mathrm{i}\omega t}$ in equations (6, 7).

### 2.1.2. *Fourier transform*

To solve equations (13, 14), we use a spatial Fourier transform defined by

$$\overline{h}(\beta, z) = \int_{-\infty}^{\infty} h(x, z)\,\mathrm{e}^{\mathrm{i}\beta t}\,\mathrm{d}x. \tag{15}$$

With the above definition of the Fourier transform, the corresponding inverse transform will include a factor $1/(2\pi)$. Now, Fourier transforming (13, 14) gives

$$\left(\frac{\mathrm{d}^2}{\mathrm{d}z^2} - \beta^2 + k_1^2 + \left(\frac{c}{c_1}\right)^2 \beta^2 - 2\omega \frac{c}{c_1^2}\beta\right)\bar{\phi} = 0, \tag{16}$$

$$\left(\frac{\mathrm{d}^2}{\mathrm{d}z^2} - \beta^2 + k_2^2 + \left(\frac{c}{c_2}\right)^2 \beta^2 - 2\omega \frac{c}{c_2^2}\beta\right)\bar{\psi} = 0. \tag{17}$$

Substituting

$$\alpha_1^2 = \beta^2 - k_1^2(1 - \beta/k)^2, \quad \alpha_2^2 = \beta^2 - k_2^2(1 - \beta/k)^2, \tag{18}$$

where $k = \omega/c$ and $k_\alpha = \omega/c_\alpha$ $\alpha = 1, 2$, one obtains the differential equations:

$$\left(\frac{\mathrm{d}^2}{\partial z^2} - \alpha_1^2\right)\bar{\phi} = 0, \quad \left(\frac{\mathrm{d}^2}{\partial z^2} - \alpha_2^2\right)\bar{\psi} = 0, \tag{19}$$

and integrating equations (19) gives

$$\bar{\phi} = \bar{A}(\beta)\mathrm{e}^{-\alpha_1 z}, \quad \bar{\psi} = \bar{B}(\beta)\mathrm{e}^{-\alpha_2 z}. \tag{20}$$

since $\Re e\{\alpha_1\} > 0$, $\Re e\{\alpha_2\} > 0$ reflections from $z = \infty$ are disallowed.

## 2.2. BOUNDARY CONDITIONS

In the transform domain, the boundary conditions (6, 7) give at $z = 0$:

$$\bar{\sigma}_z = (\lambda + 2\mu)\frac{\mathrm{d}^2\bar{\phi}}{\mathrm{d}z^2} - \lambda\beta^2\bar{\phi} + 2\mu\mathrm{i}\beta\frac{\mathrm{d}\bar{\psi}}{\mathrm{d}z}$$

$$= -P\frac{\sin(\beta b)}{\beta b}, \tag{21}$$

and

$$\bar{\tau}_{xz} = 2\mathrm{i}\beta\frac{\mathrm{d}\bar{\phi}}{\mathrm{d}z} - \beta^2\bar{\psi} - \frac{\mathrm{d}^2\bar{\psi}}{\mathrm{d}z^2}$$

$$= 0. \tag{22}$$

Hence, with some algebraic manipulations (21, 22) yield a pair of equations for $\bar{A}$ and $\bar{B}$:

$$(\alpha_2^2 + \beta^2)\bar{A} - 2i\beta\alpha_2\bar{B} = -\frac{P}{\mu}\frac{\sin(\beta b)}{\beta b}, \tag{23}$$

$$2i\beta\alpha_2\bar{A} + (\alpha_2^2 + \beta^2)\bar{B} = 0. \tag{24}$$

Thus,

$$\bar{A} = -\frac{P}{\mu}\frac{\sin(\beta b)}{\beta b}\frac{(\beta^2 + \alpha_2^2)}{\bar{F}(\beta)}, \tag{25}$$

$$\bar{B} = \frac{P}{\mu}\frac{\sin(\beta b)}{\beta b}\frac{2i\alpha_1\beta}{\bar{F}(\beta)}, \tag{26}$$

where

$$\bar{F}(\beta) = \{(\alpha_2^2 + \beta^2)^2 - 4\alpha_1\alpha_2\beta^2\}. \tag{27}$$

For $c = 0$ $\bar{F}(\beta)$ is known as the Rayleigh function. The value of the Rayleigh wave speed, $c_R$, may be deduced from the Rayleigh function (see Appendix A).

Recapping, the longitudinal and vertical displacements are represented through the Helmholtz potentials

$$u = \frac{\partial\phi}{\partial x} - \frac{\partial\psi}{\partial z}, \qquad w = \frac{\partial\phi}{\partial z} + \frac{\partial\psi}{\partial x}$$

and hence,

$$\bar{u} = [i\beta\bar{A}e^{-\alpha_1 z} + \alpha_2\bar{B}e^{-\alpha_2 z}]|_{z=0} = -\frac{iP}{\mu}\frac{\sin(\beta b)}{\bar{F}(\beta)}(\beta^2 + \alpha_2^2 - 2\alpha_1\alpha_2),$$

$$\bar{w} = [-\alpha_1\bar{A}e^{-\alpha_1 z} + i\beta\bar{B}e^{-\alpha_2 z}]|_{z=0} = -\frac{P}{\mu}\frac{\sin(\beta b)}{\beta b}\frac{\alpha_1}{\bar{F}(\beta)}k_2^2\left(\frac{\beta}{k} - 1\right)^2.$$

The displacements on the surface of the ground are then given by the inverse Fourier transform:

$$U|_{z=0} = \left\{-\frac{iP}{2\pi\mu b}\int_{-\infty}^{+\infty}\frac{\sin(\beta b)}{\bar{F}(\beta)}(\beta^2 + \alpha_2^2 - 2\alpha_1\alpha_2)e^{i\beta x}\,d\beta\right\}e^{i\omega t}, \tag{28}$$

$$W|_{z=0} = \left\{-\frac{P}{2\pi\mu}\int_{-\infty}^{+\infty}\frac{\sin(\beta b)}{\beta b}\frac{\alpha_1}{\bar{F}(\beta)}k_2^2\left(\frac{\beta}{k} - 1\right)^2 e^{i\beta x}\,d\beta\right\}e^{i\omega t}. \tag{29}$$

Note that if $c = 0$, equations (28, 29) reduce to the known expressions for a stationary harmonic vibrating strip load given by Le Houédec [13].

## 3. NUMERICAL RESULTS

The soil characteristics were chosen from a particular British Rail site at which the constants have been measured. The values used were therefore $E = 2{\cdot}69 \times 10^8\ \mathrm{N\,m^2}$, $v = 0{\cdot}257$ and $\rho = 1550\ \mathrm{kg\,m^3}$ with a loss factor for the "modified" damping model $\eta = 0{\cdot}1$, soil A in Table 1. The values of the Rayleigh, shear and compression wave speeds were $c_R = 242$ m/s, $c_2 = 263$ m/s and $c_1 = 459$ m/s respectively. Material constants and wave speeds for three other soils are tabulated in Table 1. These will be used in a parametric study in a following section. The vertical load $P$ was given the magnitude $P = 2\pi$ N/m, and the half-length $b$ was 0·75 m.

The next section describes the behaviour of the vertical response for different load speeds.

### 3.1. TRANSFORM DOMAIN RESULTS

The real part of the transformed displacements, obtained with a "modified" hysteretic damping presented in Appendix A, is plotted in Figure 2. The material properties used to plot this figure are the British Rail site parameters, soil A, Table 1. For a stationary load, ($c = 0$ m/s) Figure 2(a), the major features are peaks located at corresponding wave numbers $\beta = \pm k_R$, $\pm k_2$ and $\pm k_1$. The peak due to the shear wave, at $\beta = k_2$, is lost to the eye due to the dominating Rayleigh wave. As $c \to c_R = 242$ m/s, Figures 2(a)–2(d), the peaks in the negative wave number domain decrease in height and move toward $-\infty$. This suggests that the contribution of these peaks to waves propagating in front of the load are not significant. On the other hand, the peaks in the positive wave number domain move to 0 and *increase* in amplitude. For non-zero damping, the inverse Fourier transform can be calculated numerically. The solutions have been obtained by the well-known Fast Fourier Transform (FFT) algorithm [14]. To compute the inverse transform accurately with a discrete transform, the integrals must be truncated at sufficiently high values to avoid distortion of the results by aliasing, while the mesh of calculated function must be fine enough to well represent the details of the functions

TABLE 1

*Material properties*

| | Soil A | Soil B | Soil C | Soil D |
|---|---|---|---|---|
| $E$ (Pa) | $2{\cdot}69 \times 10^8$ | $5{\cdot}38 \times 10^8$ | $10{\cdot}76 \times 10^8$ | $2{\cdot}0 \times 10^8$ |
| $\rho$ (kg m) | 1550 | 3100 | 2000 | 1250 |
| $v$ | 0·257 | 0·257 | 0·257 | 0·257 |
| $\eta$ | 0·1 | 0·1 | 0·1 | 0·1 |
| $c_R$ (m/s) | 242 | 242 | 426 | 232 |
| $c_2$ (m/s) | 263 | 263 | 463 | 252 |
| $c_1$ (m/s) | 459 | 459 | 809 | 441 |

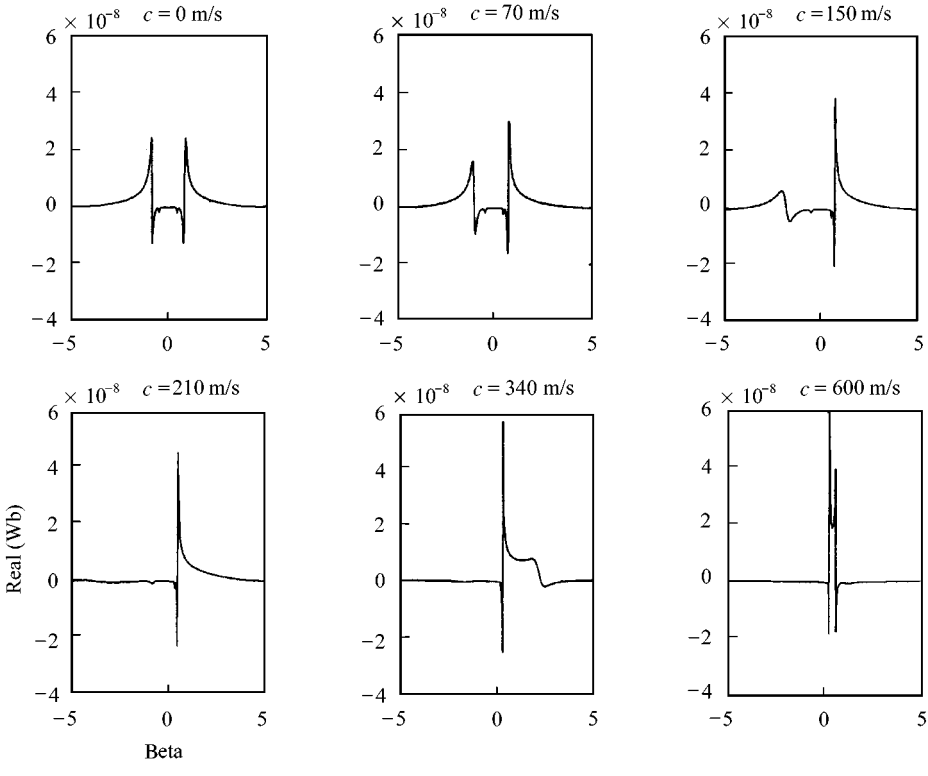


Figure 2. Evolution of the real part of transformed vertical displacements in the wave-number domain with increasing load speed.

seen in the transform domain, Figure 2. It was found that, with the material properties used here, an FFT with 8192 points and a range of $-20 \leqslant \beta \leqslant 20$ satisfied both these requirements.

### 3.2. VALIDATION AND PRELIMINARY RESULTS

The following results, for the vertical and longitudinal responses, relate to an observer moving with the strip load. The very high load speeds, up to 500 m/s, are indicative for vehicles travelling beyond wave speeds associated with the soil. Softer soils exhibit slower wave speeds close to the world record of 143 m/s. For a stationary load, $c = 0$ m/s, results were compared with those obtained by Jones and Petyt [15]. In Figure 3, results non-dimensionalized by strip length show the same solutions as in reference [15], with peak amplitude of vertical amplitude displacements, $|w|/b = 5{\cdot}82 \times 10^{-8}$, at 8 Hz. Also note, from the same figure, that the amplitude of the vertical displacement increases as the excitation frequency decreases and the response is symmetric. Increasing the load speed to $c = 200$ m/s in Figure 4, we see a slight increase in peak amplitude, namely $|w|/b = 7{\cdot}03 \times 10^{-8}$ at 8 Hz. For $c_1 > c = 400$ m/s $> c_R$, Figure 5, the responses are similar: they represent a wavefront with almost no displacement in front of the load, since the load speed is beyond the Rayleigh wave speed (see Appendix A), with a maximum

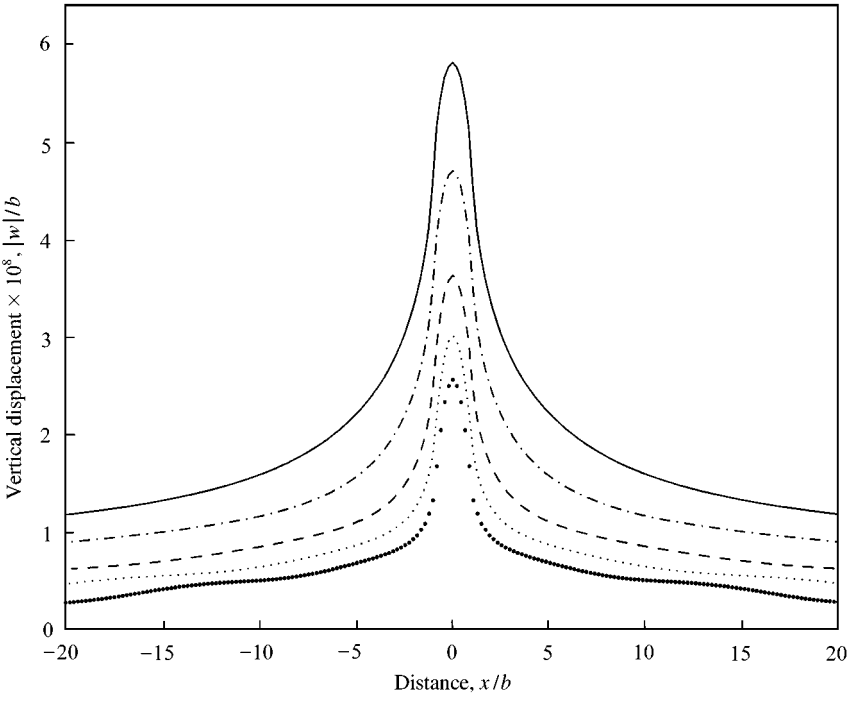


Figure 3. Non-dimensional vertical motion for stationary load, $c = 0$ m/s, for five frequencies, solid-line $f = 8$ Hz, dash–dot $f = 16$ Hz, dashed $f = 32$ Hz, light-dot $f = 48$ Hz, heavy-dot $f = 64$ Hz.

displacement at 8 Hz decreased to $|w|/b = 3{\cdot}36 \times 10^{-8}$. Increasing the load speed further, $c = 500$ m/s $> c_1 > c_R$, Figure 6, the maximum displacement is almost equivalent for all frequencies, $|w|/b = 2{\cdot}45 \times 10^{-8}$ in the neighbourhood behind the load. We can see that the influence of the load speed versus frequency, for supersonic speeds, has a minor effect in the local neighbourhood of the force. However, in comparison with Figures 3 and 4, the influence is spread over a significant distance behind the load.

### 3.3. NON-DIMENSIONAL RESULTS—PARAMETRIC STUDY

Figures 3–6 show the appearance of oscillations behind the load as the load speed increases. The apparent wavelength of these oscillations depends on both frequency and speed of the load. The following parametric study investigates the factors which describe this phenomenon.

#### 3.3.1. *Soil characteristics*

In this part, the influence of the soil characteristics is studied by comparing results obtained for four different soils. The parameters of each soil are presented in Table 1. From Figure 7, we can see that the maximum amplitude, non-dimensionalized against appropriate Rayleigh wavelength, $|w|/\lambda_R$ at a frequency $f = 64$ Hz varies with different soil parameters. However, the apparent

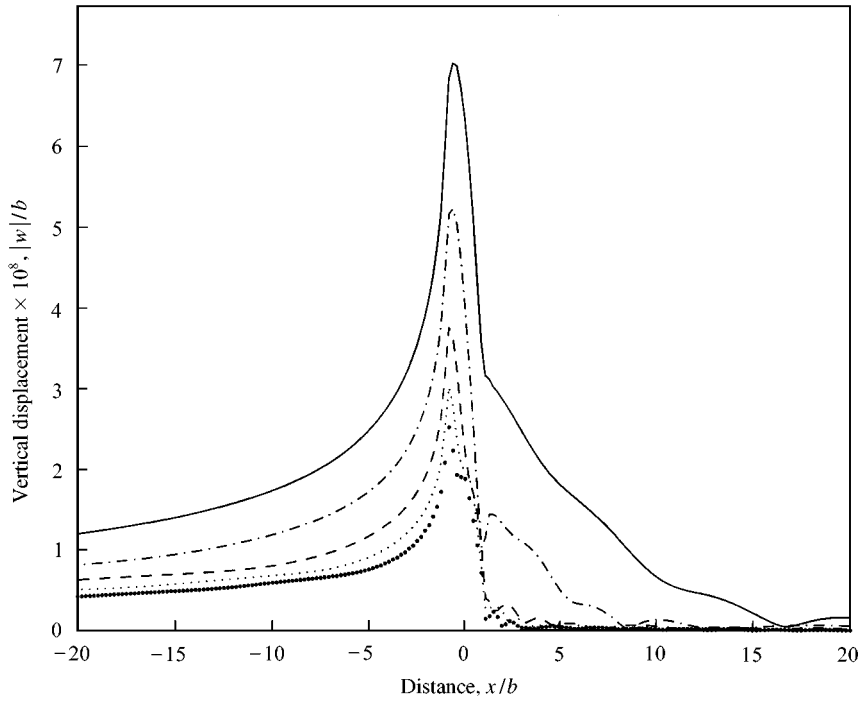


Figure 4. Non-dimensional vertical motion for load speed, $c_R > c = 200$ m/s, for five frequencies, solid-line $f = 8$ Hz, dash–dot $f = 16$ Hz, dashed $f = 32$ Hz, light–dot $f = 48$ Hz, heavy-dot $f = 64$ Hz.

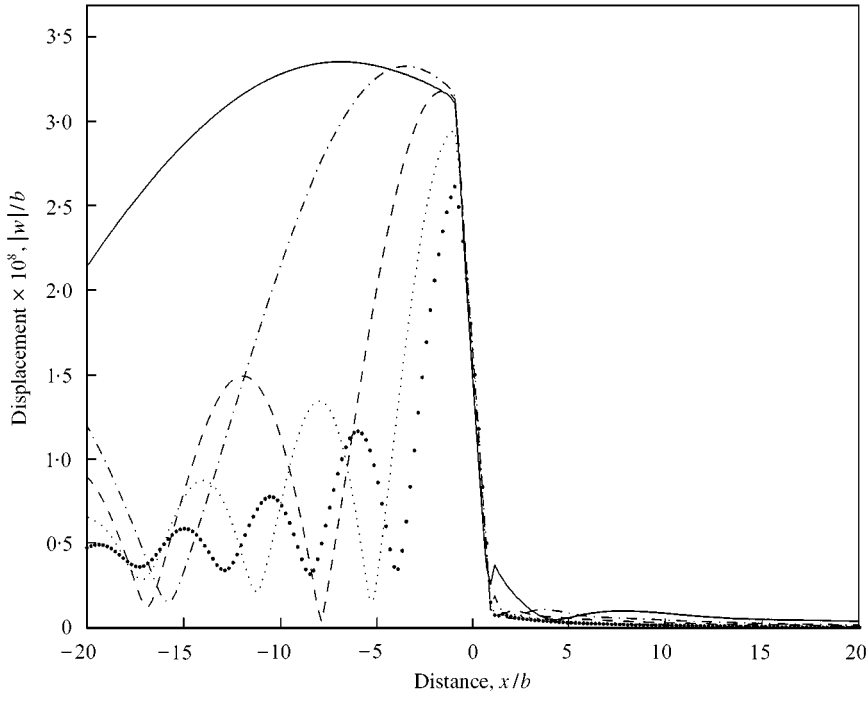


Figure 5. Non-dimensional vertical motion for load speed, $c = 400 > c_R$ m/s, for five frequencies, solid-line $f = 8$ Hz, dash–dot $f = 16$ Hz, dashed $f = 32$ Hz, light–dot $f = 48$ Hz, heavy-dot $f = 64$ Hz.

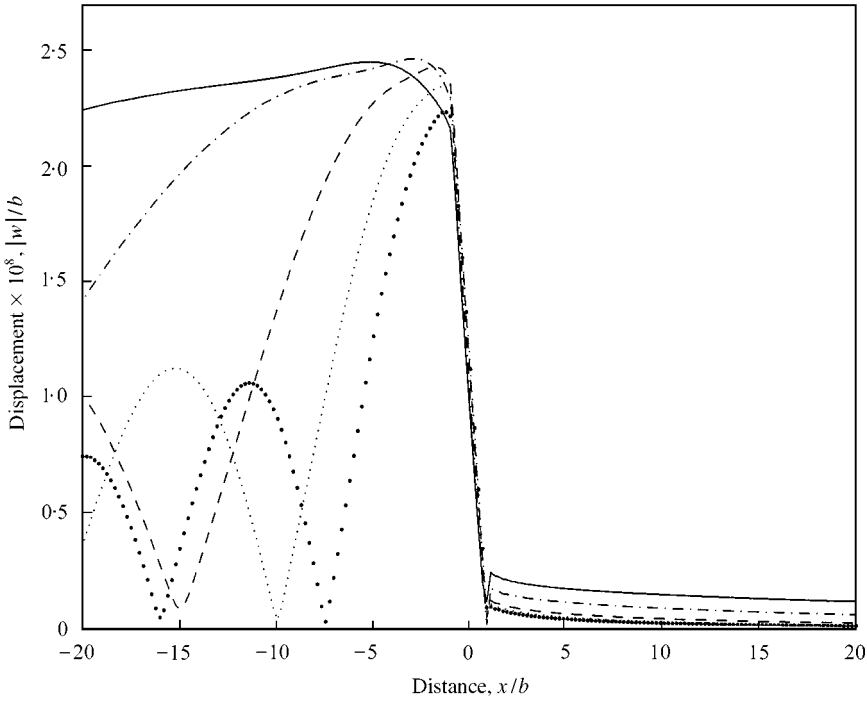


Figure 6. Non-dimensional vertical motion for load speed, $c = 500 > c_1$ m/s, for five frequencies, solid-line $f = 8$ Hz, dash–dot $f = 16$ Hz, dashed $f = 32$ Hz, light–dot $f = 48$ Hz, heavy-dot $f = 64$ Hz.

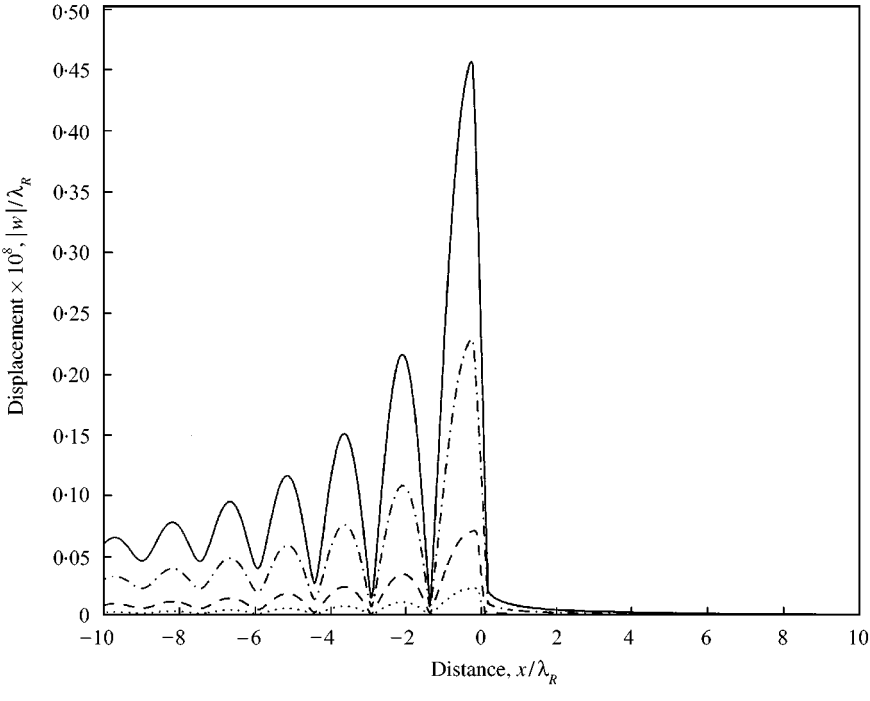


Figure 7. Non-dimensional vertical motion for four soil material parameters at load speed $c = 2c_R$, solid-line soil A, dash–dot soil B, dashed soil C, light-dot soil D.

"wavelength" of oscillation is the same for all soil types, which will only be true for displacements over a half-space due to the dominant nature of the Rayleigh wave, Ewing *et al.* [16]. For this reason, only the material parameters for one type of soil (soil A), were subsequently used.

### 3.3.2. *Load characteristics*

Although it is not shown here, the half-length of the strip load, $b$, has no influence on the apparent "wavelength" of oscillation. Figure 8 shows that for different values of frequency, the general form of vertical amplitude of the displacement, $|w|/\lambda_R$ versus $x/\lambda_R$ is the same, only amplitudes of displacements change. Note that non-dimensional displacements increase with frequency.

Increasing the load speed, $M_R = c/c_R$ from stationary, such that $0 < M_R \leqslant 1$, with $f = 64$ Hz, leads to a slight perturbation of the amplitude of vertical displacements, $|w|/\lambda_R$ behind the load but an abrupt change in front of the load, Figure 9. For high Mach numbers, $M_R > 1$, oscillations appear behind the load with increasing apparent "wavelength" as $M_R$ increases, Figure 10. In Figure 11, the non-dimensional vertical displacements are plotted against $x/(\lambda_R(M_R^2 - 1))$; which shows that the "wavelength" of the vibrations of displacements behind the load is directly proportional to this factor, similar to results obtained in acoustics, Morse and Ingard [17].

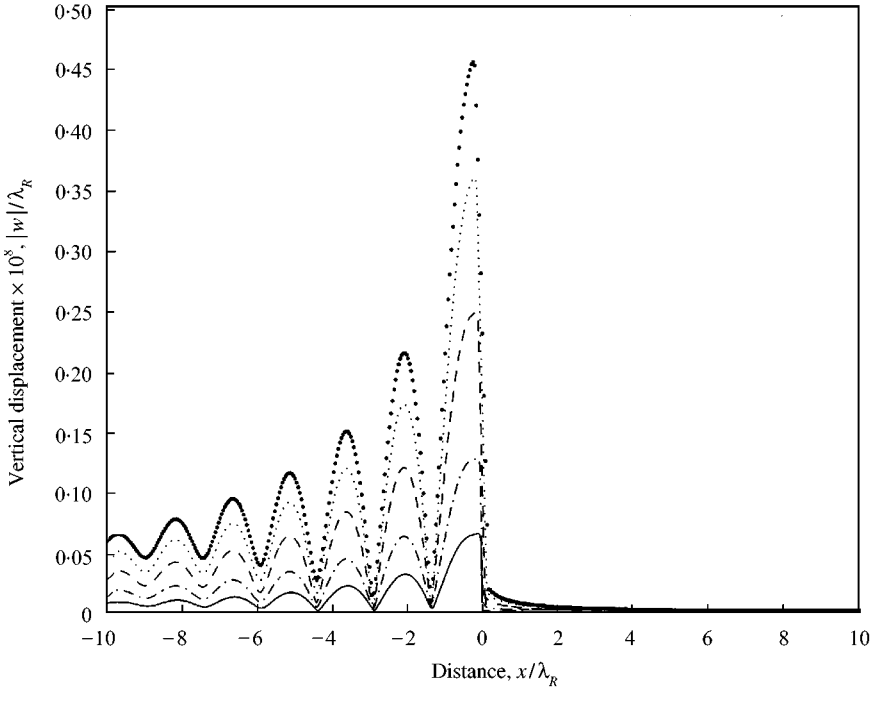


Figure 8. Non-dimensional vertical motion at load speed $c = 2c_R$, for five frequencies, solid-line $f = 8$ Hz, dash–dot $f = 16$ Hz, dashed $f = 32$ Hz, light-dot $f = 48$ Hz, heavy-dot $f = 64$ Hz.

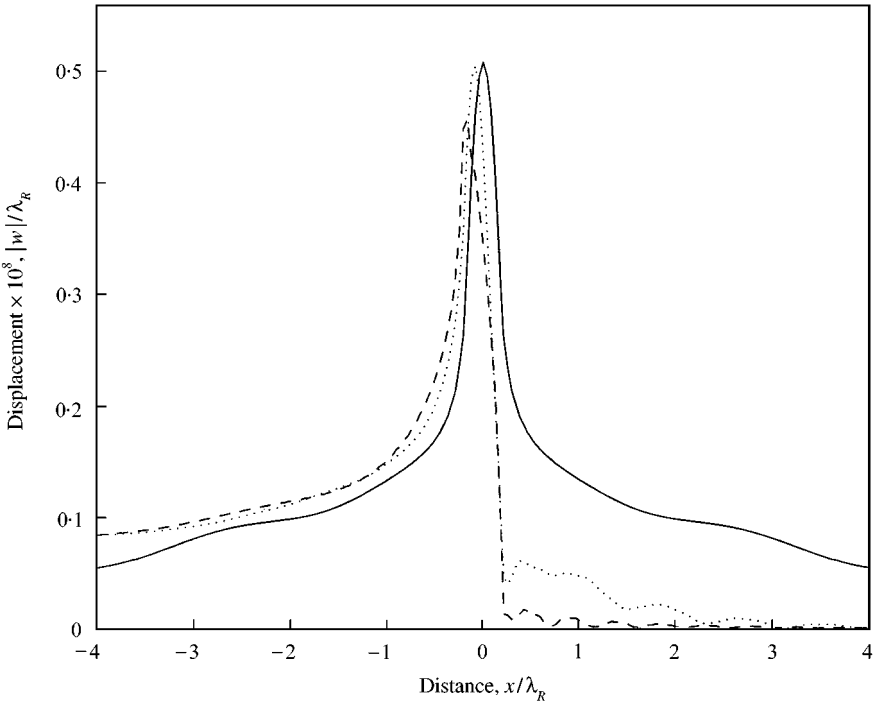


Figure 9. Non-dimensional vertical motion at frequency $f = 64$ Hz for three load speeds, solid-line $c = 0$ m s, dash–dot $c = c_R/2$, dashed $c = c_R$.

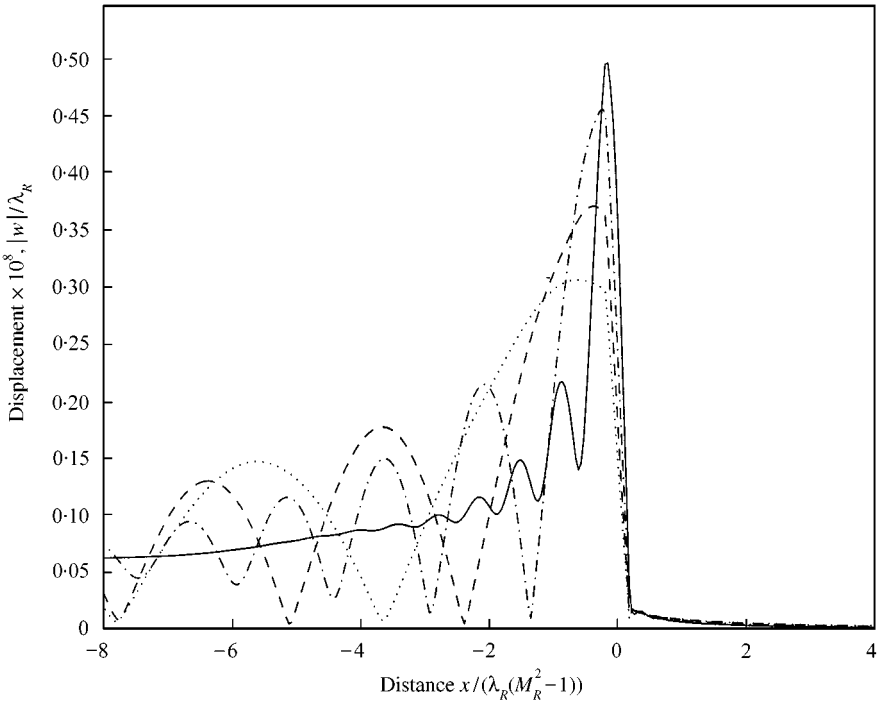


Figure 10. Non-dimensional vertical motion at frequency $f = 64$ Hz for four load speeds, solid-line $c = 3c_R/2$, dash–dot $c = 2c_R$, dashed $c = 5c_R/2$, light-dot $c = 3c_R$.

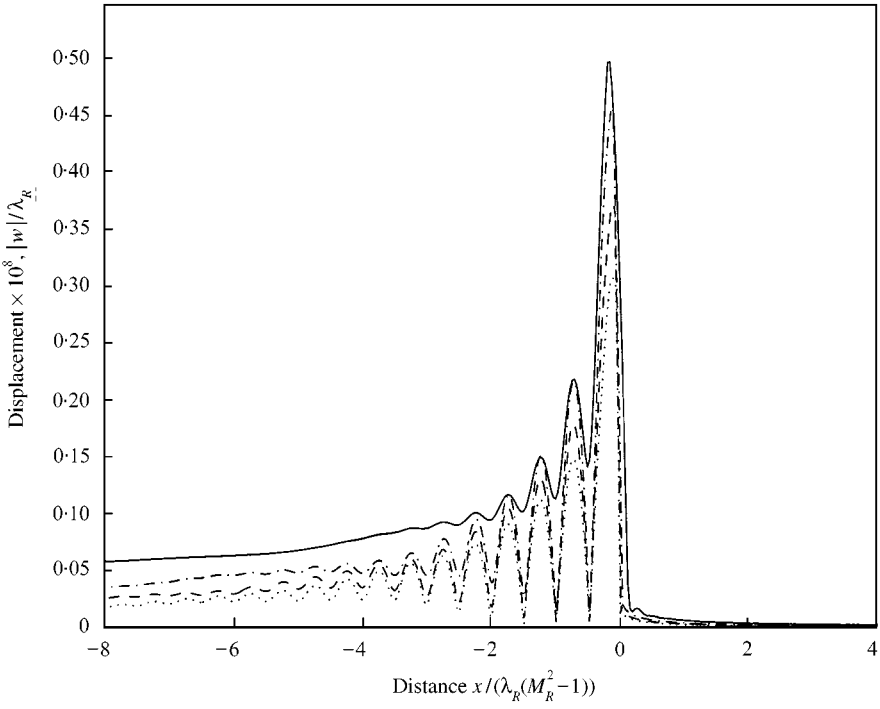


Figure 11. Non-dimensional vertical motion at frequency $f = 64$ Hz for four load speeds, solid-line $c = 3c_R/2$, dash–dot $c = 2c_R$, dashed $c = 5c_R/2$, light-dot $c = 3c_R$ with the space variable non-dimensionalized by $x/(\lambda_R(M_R^2 - 1))$.

A similar study for longitudinal displacements lead to the same conclusions, see Figure 12. Values of the amplitude of longitudinal displacements are generally lower than those of vertical displacements. The maximum amplitude of longitudinal displacement increases from $|u|/\lambda_R = 1{\cdot}38 \times 10^{-9}$ in the immediate vicinity away from the load, at $M_R = 0$, to $|u|/\lambda_R = 1{\cdot}77 \times 10^{-9}$ at the trailing edge of the load ($x = -b$).

### 3.3.3. *Conclusions from the parametric study*

In the supersonic regime, $c > c_R$, it is shown that two Rayleigh waves propagate behind the load generating a resultant wave, Figures 10 and 11. It is evident that the only material parameter which affects the apparent "oscillation" of the resultant wave is the Mach number $M_R$. Thus, if we denote by $\lambda^*$ the "period" of non-dimensional oscillations and by $\hat{\lambda}$ the wavelength of the actual vertical displacements, we observe:

$$\lambda^* = \frac{\hat{\lambda}}{\lambda_R} = \frac{1}{2}(M_R^2 - 1), \quad \text{and hence } \hat{\lambda} = \frac{\pi(c^2 - c_R^2)}{\omega c_R} = \frac{2\pi}{\beta_2 - \beta_2}, \tag{30}$$

where $\beta_1$ and $\beta_2$ are the positions of the Rayleigh poles, see Appendix A. From Appendix A it is seen that the wavelength of the resultant wave is a combination of

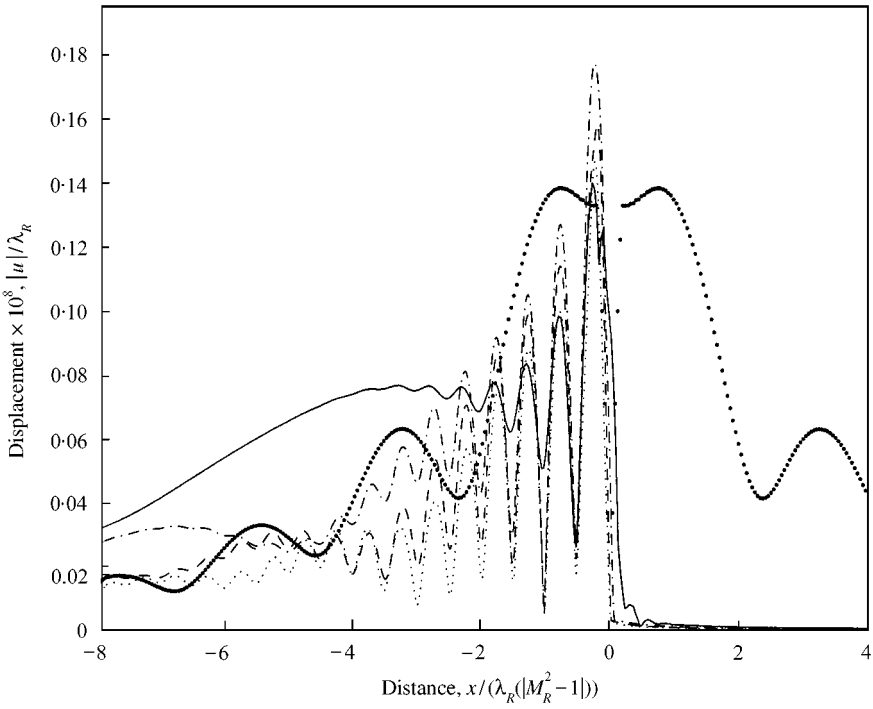


Figure 12. Non-dimensional longitudinal motion at frequency $f = 64$ Hz for five load speeds, heavy-dot $c = 0$ m/s, solid-line $c = 3c_R/2$, dash–dot $c = 2c_R$, dashed $c = 5c_R/2$, light-dot $c = 3c_R$ with the space variable non-dimensionalized by $x/(\lambda_R(M_R^2 - 1))$.

the two Rayleigh wavelengths. Since the dominant wave on the surface of a half-space is the Rayleigh wave [16] this justifies the observation (30) being consistent with the analysis in Appendix A.

The wavelength of displacements, $\hat{\lambda}$, depends on three factors: the Rayleigh wave speed $c_R$, the load speed $c$ and its excitation $\omega$, $\lambda^*$ depends on one factor, the Mach number $M_R$. This justifies the interest of the factor $1/(\lambda_R(M_R^2 - 1)$ in the supersonic region.

### 3.4. INFLUENCE OF DEPTH OBSERVATION

The amplitude of displacements decreases with depth, as shown in Figures 13 and 14 in which contour levels of vertical displacements are plotted. For a fixed load, the response is symmetric, see Figure 13. For high load speeds, two different zones appear behind the load, delineated by two lines, see Figure 14. These are called the Mach lines; the first one is due to the $P$ wave ($P$-line) and the second the $S$ wave ($S$-line). The displacements are contained within the surface of the ground and the $P$-line. These results agree, in form, with those of De Barros and Luco [8], who have shown for high load speeds, that an abrupt discontinuity along $P$- and $S$-line appears behind the load. Krylov [11], has also shown that displacements are contained in a cone behind the load in the supersonic region.

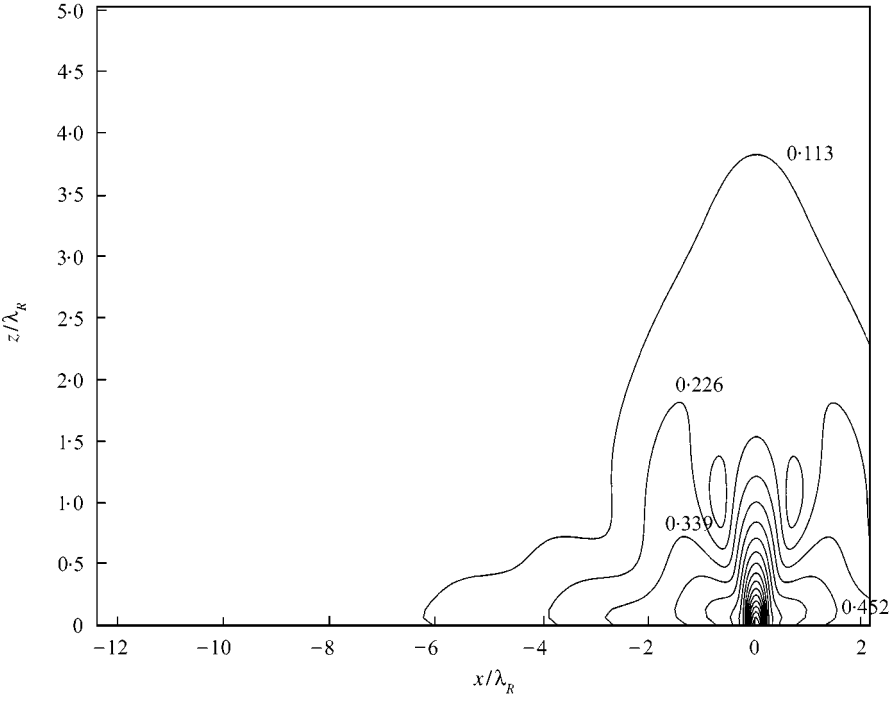


Figure 13. Contours of vertical motion $|w| \times 10^8$, below surface of the half-space for a stationary load and frequency $f = 64$ Hz. Contour values are $|w|/\lambda_R \times 10^{-9}$.

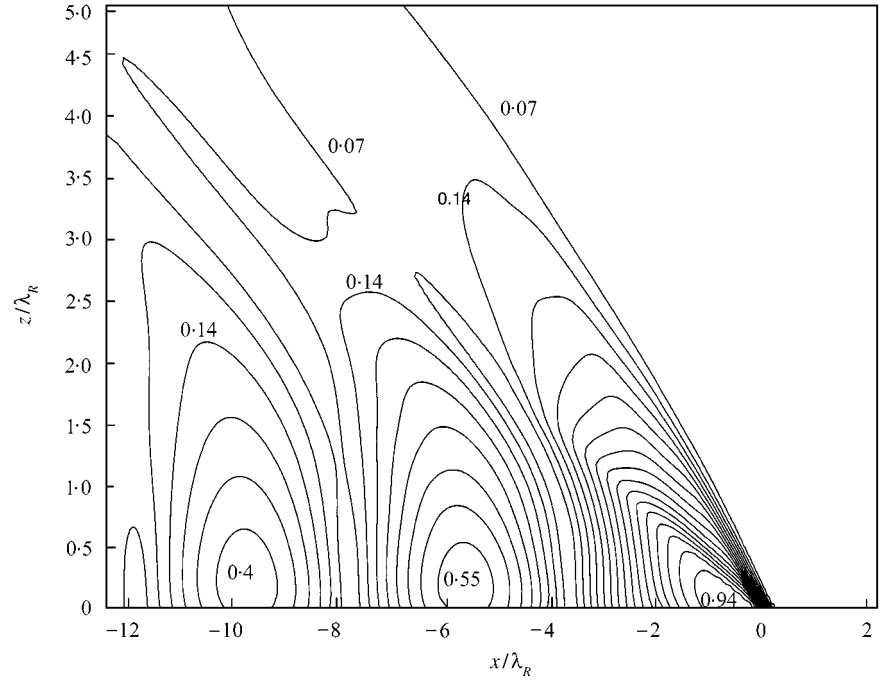


Figure 14. Contours of vertical motion $|w| \times 10^8$, below surface of the half-space at speed $c = 3c_R$. and frequency $f = 64$ Hz. Contour values are $|w|/\lambda_R \times 10^{-9}$.

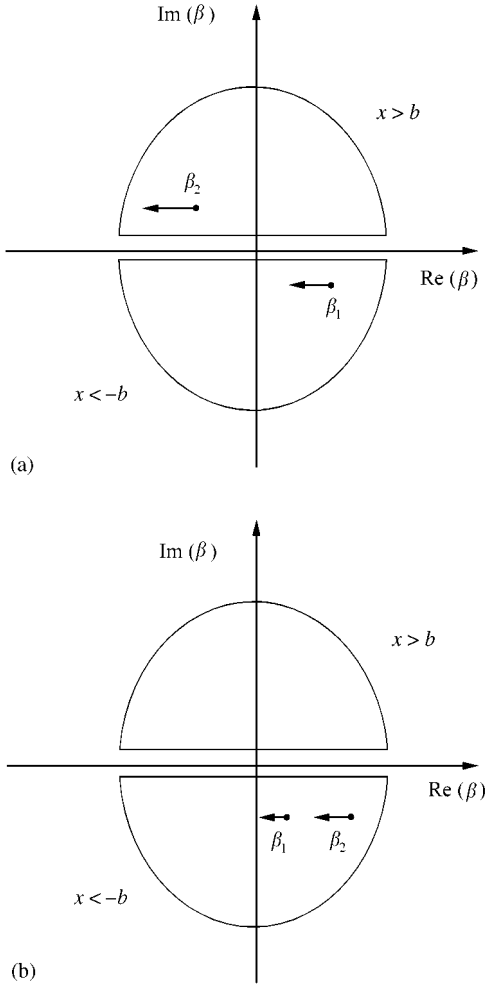


Figure 15. Location of the Rayleigh poles, $\beta_1$ and $\beta_2$ and typical complex integration contours, (a) for $c < c_R$ and (b) for $c > c_R$.

## 4. CONCLUSIONS

A two-dimensional semi-analytic model of ground vibration due to a moving harmonic strip load has been developed. The model consists of an elastic, isotropic and homogeneous half-space, with modified hysteretic damping, excited by a uniform harmonic surface load moving with constant speed. The equations of motion were solved with the aid of the Fourier Transform, the inverse transformation being performed with the inverse FFT. The contribution of the Rayleigh poles was studied in the transformed wave-number domain, showing the existence of a Doppler effect in the subsonic case. Results presented show the behaviour of the transformed vertical components in the wave-number domain, and vertical displacements for a range of speeds and excitation frequencies. As the load speed of the vertical strip load advanced beyond the Rayleigh wave speed, a shock cone develops behind the load confined to the region between the shock fronts.

## ACKNOWLEDGMENTS

This work has been partly carried out under EPSRC grants GR/H39895 and GR/L11397 and a French–British Alliance grant. Gaëlle Lefeuve-Mesgouez and Andrew Peplow acknowledge the support of the British Council and the APAPE who provided a French–British research grant.

## REFERENCES

1. G. Eason, J. Fulton and I. N. Sneddon 1956 *Philisophical Transactions of the Royal Society* **A248**, 575–607. Generation of waves in an infinite elastic solid by variable body-forces.
2. G. Eason 1965 *International Journal of Engineering Science* **2**, 581–609. The stress produced in a semi-infinite solid by moving surface force.
3. J. Cole and J. Huth 1958 *Journal of Applied Mechanics* **25**, 433–436. Stresses produced in a half-plane by moving loads.
4. H. G. Georgiadis and J. R. Barber 1993 *Journal of Applied Mechanics* **60**, 772–774. Steady-state transonic motion of a line load over an elastic half-space: the corrected Cole/Huth solution.
5. L. Fryba 1972 *Vibration of Solids and Structures Under Moving Loads*, *Mechanics of Structural Systems*. Groningen: Noordhoff International Publishing.
6. L. M. Keer 1969 *The Journal of the Acoustical Society of America* **47**, 1359–1365. Moving and simultaneously fluctuating loads on an elastic half-plane.
7. M. Gunaratne and O. Sanders 1996 *International Journal for Numerical and Analytical Methods in Geomechanics* **20**, 191–208. Response of a layered elastic medium to a moving strip load.
8. F. C. P. De Barros and J. E. Luco 1995 *Applied Mathematics and Computation* **67**, 103–134. Stresses and displacements in a layered half-space for a moving line load.
9. R. G. Payton 1967 *International Journal of Engineering Sciences* **5**, 49–79. Transient motion of an elastic half-space due to a moving surface line load.
10. F. C. P. De Barros and J. E. Luco 1994 *Wave Motion* **19**, 189–210. Response of a layered viscoelastic half-space to a moving point load.
11. V. V. Krylov 1995 *Applied Acoustics* **44**, 149–164. Generation of ground vibrations by superfast trains.
12. D. V. Jones, D. Le Houédec, A. T. Peplow and M. Petyt 1998 *European Journal of Mechanics A/Solids* **17**, 153–166. Vibration in the vicinity of a moving harmonic rectangular load on a half-space.
13. D. Le Houédec 1980 *Thèse de Doctorat ès Sciences*, *Université de Nantes*. Réduction et propagation dans le sol des vibrations dues au trafic routier urbain: cas particulier des chaussées sur fondation élastique.
14. E. O. Brigham 1974 *The Fast Fourier Transform*. Englewood Cliffs, NJ: Prentice-Hall.
15. D. V. Jones and M. Petyt 1991 *Journal of Sound and Vibration* **147**, 155–166. Ground vibration in the vicinity of a strip load: a two-dimensional model.
16. W. M. Ewing, W. S. Jardetzky and F. Press 1957 *Elastic Waves in layered Media*. New York: McGraw-Hill.
17. P. M. Morse and K. U. Ingard 1986 *Theoretical Acoustics*. New York: McGraw-Hill.

## APPENDIX A: ANALYSIS OF MODIFIED DAMPING MODEL

For the purpose of numerical integration it is worth examining the Rayleigh function $\bar{F}(\beta)$ (27) for zero damping, $\eta = 0$. By tracking the location of poles and branch points for various load speeds, in the complex plane, the dominant features

of the solution may be determined. Writing the Rayleigh function in full:

$$\bar{F}(\beta) = \beta^4 \left\{ \left( 2 - \frac{k_2^2}{\beta^2}\left(1 - \frac{\beta}{k}\right)^2 \right)^2 - 4\left(1 - \frac{k_1^2}{\beta^2}\left(1 - \frac{\beta}{k}\right)^2\right)^{1/2} \left(1 - \frac{k_2^2}{\beta^2}\left(1 - \frac{\beta}{k}\right)^2\right)^{1/2} \right\} \tag{A1}$$

and the Rayleigh function, $F_R$ [13], for a stationary harmonic force:

$$F_R(k_R) = \left(2 - \frac{k_2^2}{k_R^2}\right)^2 - 4\left(1 - \frac{k_1^2}{k_R^2}\right)^{1/2} \left(1 - \frac{k_2^2}{k_R^2}\right)^{1/2} \tag{A2}$$

from which the Rayleigh wave speed, $c_R$, and Rayleigh wave number, $k_R = \omega/c_R$, may be calculated.

Comparing equations (A1) and (A2) we see that the poles in the $(c, \beta)$-plane satisfy the equation.

$$\left(1 - \frac{\beta}{k}\right)^2 = \frac{\beta^2}{k_R^2}. \tag{A3}$$

Therefore, the poles lie on the two curves, $\beta_1$ and $\beta_2$, where

$$\beta_1 = \frac{\omega}{(c + c_R)} \quad \text{and} \quad \beta_2 = \frac{\omega}{(c - c_R)} \tag{A4}$$

It is easy to see, from equation (A1), that branch points lie on the same curves with $k_R, c_R$ replaced with $k_1, c_1$ or $k_2, c_2$.

The nature of the vertical and longitudinal displacements on the surface of the half-space is dominated by the Rayleigh wave as the load speed increases beyond the propagating speed of this surface wave. The next section gives some insight into the choice of damping model necessary in this study.

### A.1. ANALYSIS OF RAYLEIGH WAVE CONTRIBUTION WITH DAMPING MODEL

For a stationary load a hysteretic damping model, where the material exhibits damping characterized by a loss factor $\eta$, may be used. The complex Lamé constants will be given by

$$\lambda = \frac{vE(1 + i\eta)}{(1 + v)(1 + 2v)}, \qquad \mu = \frac{E(1 + i\eta)}{2(1 + v)}. \tag{A5}$$

A standard hysteretic damping model (A5), is not suitable for the moving load problem as will be demonstrated in the following section (see the remark after equation (A11)).

For a moving load problem it is necessary to modify the standard damping model. If we write a modified hysteretic damping model through material damping

with a factor $(1 + i\eta f(k, \beta_m))$, $m = 1, 2$, where

$$f(k, \beta_m) = \text{sign}(k - \beta_m), \quad m = 1, 2 \tag{A6}$$

for small values of $0 < \eta \ll 1$, where $k = \omega/c$, the poles will be situated just off the real-line in the complex plane. The first pole, $\beta_1$ is located at

$$\beta_1 \approx \frac{\omega(c + c_R) - i\omega c_R \eta f(k, \beta_1)/2}{(c + c_R)^2 + c_R^2 \eta^2/4}, \tag{A7}$$

and the second pole at

$$\beta_2 \approx \frac{\omega(c - c_R) + i\omega c_R \eta f(k, \beta_2)/2}{(c - c_R)^2 + c_R^2 \eta^2/4}. \tag{A8}$$

Specifically, for the sub-Rayleigh and super-Rayleigh cases:

(i) *Sub-Rayleigh case*: $(c < c_R)$. The poles are located at

$$\beta_1 \approx \frac{\omega(c + c_R) - i\omega c_R \eta/2}{(c - c_R)^2 + c_R^2 \eta^2/4} \quad \text{and} \quad \beta_2 \approx \frac{\omega(c - c_R) + i\omega c_R \eta/2}{(c - c_R)^2 + c_R^2 \eta^2/4} \tag{A9}$$

as shown in Figure 15(a).

(ii) *Sub-Rayleigh case*: $(c > c_R)$. The poles are now located at

$$\beta_1 \approx \frac{\omega(c + c_R) - i\omega c_R \eta/2}{(c + c_R)^2 + c_R^2 \eta^2/4} \quad \text{and} \quad \beta_2 \approx \frac{\omega(c - c_R) - i\omega c_R \eta/2}{(c - c_R)^2 + c_R^2 \eta^2/4} \tag{A10}$$

as shown in Figure 15(b).

Similarly, the branch points swap imaginary signs as the load speed increases beyond the shear-wave speed, $c_1$, and compressive-wave speed, $c_2$. The choice of this damping model is evident through examination of the propagating Rayleigh waves.

For a certain load speed, $c$ and zero damping, the two poles, $\beta_1$ and $\beta_2$, of the Rayleigh function $\bar{F}(\beta)$ (A1), are real, and are given in equation (A4). As the load speed, $c > 0$, increases, the position of pole, $\beta_1$, moves continuously from $\beta_1 = k_R$ to $\beta_1 = 0$ as $c \to \infty$. However, the position of pole, $\beta_2$, moves from $\beta_2 = -k_R$ to $\beta \to -\infty$ as $c \to c_R$. Beyond the Rayleigh wave speed, the position of the pole moves from $\beta_2 = +\infty$ to 0. The contributions to the vertical displacement by the onset of propagating waves for the two regions of interest, $c < c_R$ and $c > c_R$ are outlined below.

(i) *Sub-Rayleigh case*: $(c < c_R)$ poles positions given by equations (A9). By contour integration in the complex plane, the contribution for $x > b > 0$ is given by the

pole in the upper-half-plane, whereas for $x < -b < 0$, it is given by the pole in the lower-half-plane.

(a) For $x > b$, $w|_{z=0} \propto Res(\beta_2) = \bar{w}(\beta_2)(\bar{F}(\beta_2)/\bar{F}'(\beta_2))\ e^{(i\beta_1 x)}$. Thus, the vertical displacements have an observed wavelength of $\beta_2^{-1} = (c_R - c)/\omega$ and the wave propagates in the positive $x$ direction.

(b) For $x < -b$, $w|_{z=0} \propto Res(\beta_1) = \bar{w}(\beta_2)(\bar{F}(\beta_1)/\bar{F}'(\beta_1))\ e^{(i\beta_2 x)}$. Thus, the vertical displacements have an observed wavelength of $\beta_1^{-1} = (c_R - c)/\omega$ and the wave propagates in the positive $x$ direction.

This is analogous to the Doppler effect in acoustics [17].

(ii) *Super-Rayleigh case*: ($c > c_R$) poles positions given by equations (A10). By contour integration the contribution for $x > b$ is given by the pole in the upper-half-plane (there are none), hence

(a) for $x > b$, $w|_{z=0} = 0$.

Similarly, for $x < -b$, the contribution is given by the poles in the lower-half-plane, hence,

(b) for $x < -b$,

$$w|_{z=0} \propto Res(\beta_1) + Res(\beta_2)$$

$$\propto \bar{w}(\beta_1)\frac{\bar{F}(\beta_1)}{\bar{F}'(\beta_1)}e^{(i\beta_1 x)} + \bar{w}(\beta_2)\frac{\bar{F}(\beta_2)}{\bar{F}'(\beta_2)}e^{(i\beta_2 x)}. \tag{A11}$$

**Remark.** Note that in (ii) (a) a pole in the upper half-plane will exist for the standard hysteretic damping model (A5). Similarly, for the branch points. Thus, an erroneous vertical displacement will appear in front of the load.

The displacements are composed of the superposition of two waves propagating in the negative $x$ direction at speeds ($c + c_R$) respectively. An interesting feature of the supersonic field is the interference between these contributions. These waves, which have different wavelengths and amplitudes give rise to a vertical displacement amplitude which oscillates with space, $x = x_1 - ct$, the space–time variable, with an apparent period equal to $2\pi/(\beta_2 - \beta_1)$. This is analogous to results obtained in acoustics [17].